Analysis of the Phase-Shifted Carrier Modulation for Modular Multilevel Converters

Binbin Li, Rongfeng Yang, Dandan Xu, Gaolin Wang, *Member, IEEE*, Wei Wang, and Dianguo Xu, *Senior Member, IEEE*

***Abstract*—The modular multilevel converter (MMC) is an emerging topology for high-power applications and is considered as the development trend of the high-voltage power converters. In this paper, general implementation of the phase-shifted carrier (PSC) modulation with a capacitor voltage balancing method for MMC is first introduced. Then, the mathematical analysis of PSC modulation for MMC is performed to identify the PWM harmonic characteristics of the output voltage and the circulating current. Moreover, influence of the carrier displacement angle between the upper and lower arms on these harmonics is also studied. Using this analysis, the optimum displacement angles are specified for the output voltage harmonics minimization and the circulating current harmonics cancellation, respectively. The harmonic features of the line-to-line voltage and the dc-link current are also investigated. Moreover, an extension of the PSC modulation for MMC with full-bridge submodules is also proposed which can increase the equivalent switching frequency of the output voltage and circulating current by two times compared with the conventional MMC. Finally, the findings are verified experimentally on a prototype of MMC.**

***Index Terms*—Fourier series, modular multilevel converter (MMC), phase-shifted carrier (PSC), pulsewidth modulation (PWM).**

I. Introduction

NOWADAYS, the increasing concerns about climate change and the growing demand for electricity have posed new challenges for power generation and transmission [1]–[3]. As an innovative and highly efficient solution for energy conversion, the modular multilevel converter (MMC) is gaining more and more attentions because it presents great advantages compared with conventional two-level or three-level voltage source converters. These advantages such as lower losses, reduced EMI noise, less semiconductor device stress, scalability and easy assembling, and the nearly ideal sinusoidal-shaped output waveforms make MMC the most attractive topology for high-voltage high-power applications, particularly in the high-voltage direct current transmission (HVDC) sector [4]–[8].

Many academic papers have been published to improve the performances of MMC. In [9]–[16], the mathematical analysis, modeling methodologies, and the semiconductor requirements of MMC under different operating conditions were carried out. The capacitor voltage balancing and circulating current suppression are two major tasks associated with MMC and several control solutions based on feedback control or the sorting algorithm have been proposed and reported in [17]–[23]. In addition, as one of the most interesting topics, various pulsewidth modulation (PWM) techniques have been developed to fit MMC. The nearest level control (NLC), also known as the round method, was adopted in [11], [24], and [25]. This method is especially suitable for MMC with a large number of submodules (SMs). Furthermore, [16] and [26] extend the application scope of NLC by introducing one SM working in PWM operation. A phase-disposition (PD) level shifted PWM strategy including a voltage balancing method was discussed in [27] and [28]. Particularly, it must be pointed out that the PD-PWM is not very preferred for MMC, as it causes an uneven power distribution among the different SMs [29]. Another popular PWM technique is the phase-shifted carrier (PSC), which is the most commonly used method in the cascaded H-bridge converters (CHB) [29]–[31]. The PSC modulation is also attractive to MMC as it has some distinctive features:

1) The semiconductor stress and the power handled by each SM are evenly distributed. Hence, the capacitor voltage balancing control can be easily achieved.
2) The output voltage has a high resulting switching frequency and a low total harmonic distortion (THD).
3) Consistent with the structure of MMC, each triangular carrier associated to a particular SM presents the nature of modularity and scalability.

Due to the aforementioned merits, the PSC scheme of CHB has been directly employed to MMC by many researchers in [18]–[23], and [32]–[34] that the carriers for SMs in the same phase are arranged with an equal phase shifts in angle. There are, however, significant differences between these two topologies. For the case of the CHB, a large number of isolated dc sources are required when transferring active power, which have to be fed from phase-shifting isolation transformers and multiphase rectifiers, which are very expensive and bulky [29]. In contrast, MMC eliminates the bulky phase-shifting transformers and has an additional dc terminal formed by the upper and lower arms, which allows bi-directional power flow between ac and dc sides. Additionally, the output voltage and circulating current of MMC

Manuscript received August 10, 2013; revised October 29, 2013 and December 10, 2013; accepted January 2, 2014. Date of publication January 13, 2014; date of current version August 26, 2014. This work was supported by National Natural Science Foundation of China under Grant 51237002 and by grants from the Power Electronics Science and Education Development Program of Delta Environmental and Educational Foundation. Recommended for publication by Associate Editor M. A. Perez.

The authors are with the School of Electrical Engineering and Automation, Harbin Institute of Technology, Harbin 150001, China (e-mail: libinbinhit@126.com; yrf@hit.edu.cn; dan_danzai@163.com; WGL818@hit.edu.cn; wangwei602@hit.edu.cn; xudiang@hit.edu.cn).

Color versions of one or more of the figures in this paper are available online at http://ieeexplore.ieee.org.

Digital Object Identifier 10.1109/TPEL.2014.2299802

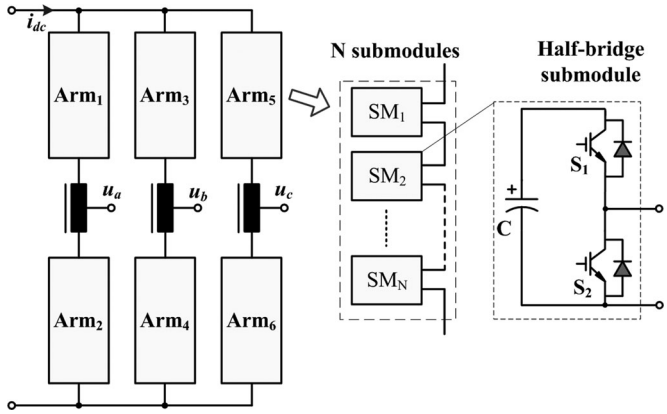

Fig. 1. Circuit configuration of the MMC.

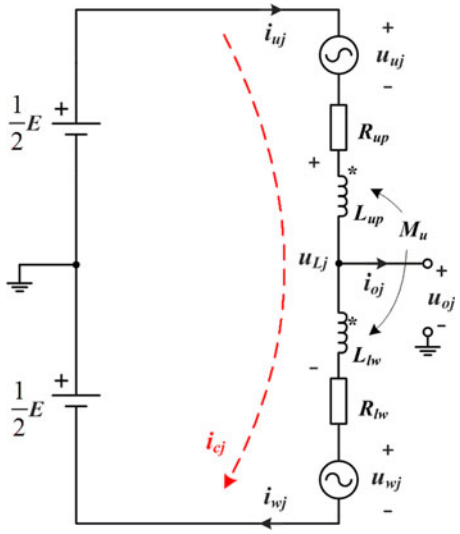

Fig. 2. Equivalent circuit of one phase of the MMC.

are determined by the interactions between the upper and the lower arm voltages [9]. Hence, when applying PSC modulation to MMC, carriers for SMs in the lower arm and carriers for SMs in the upper arm need to be considered separately, with an interleaved displacement angle. This displacement angle will affect the high-frequency interactions between the upper and lower arms, and further determines the harmonic features of MMC.

So far, few studies have analyzed the principle of PSC modulation for MMC and it remains unclear how the displacement angle would influence the performance of MMC. It is, therefore, the aim of this paper to provide a fully mathematical analysis of the PSC modulation implemented in MMC, to investigate the impact of the displacement angle on the voltage and current harmonics, and to find out an optimal displacement angle which can minimize these harmonics.

The rest of this paper is organized as follows. Section II introduces the circuit configuration and mathematical model of MMC. Section III provides the implementation of PSC modulation to MMC combined with a capacitor voltage balancing method. In Section IV, the output voltage harmonics minimization PSC scheme and the circulating current harmonics cancellation PSC scheme are proposed based on the Fourier series analysis. Furthermore, Section V extends the PSC modulation method to MMC with full-bridge SMs. The validity of the analysis and the proposed PSC schemes are verified by experimental results on a three-phase MMC prototype in Section VI. Finally, Section VII summarizes this paper.

II. Basic Operating Principles

A. Structure of MMC

The circuit configuration of a three-phase MMC is shown in Fig. 1. Each phase of MMC consists of two arms, the upper and the lower, which are connected through buffer inductors. Each arm is formed by a series connection of N nominally identical half-bridge SMs and each SM contains a dc capacitor and two insulated gate bipolar transistors (IGBTs). The single coupled inductor is preferred in this paper as it has smaller size and lighter weight than the total of the two separate inductors [5].

B. Mathematical Model of MMC

As shown in Fig. 2, the equivalent circuit diagram of one phase of MMC is used for analysis. u_{oj} is the output voltage of phase j ($j \in \{a, b, c\}$), i_{oj} is the phase current, and E is the dc-link voltage. u_{uj}, i_{uj} and u_{wj}, i_{wj} represent the voltages and currents of the upper arm and the lower arm, respectively.

The following equations can be obtained by Kirchhoff's voltage law:

$$R_{\rm up} i_{uj} + L_{\rm up} \frac{di_{uj}}{dt} + M_u \frac{di_{wj}}{dt} = \frac{E}{2} - u_{uj} - u_{oj} \quad (1)$$

$$R_{lw} i_{wj} + L_{lw} \frac{di_{wj}}{dt} + M_u \frac{di_{uj}}{dt} = \frac{E}{2} - u_{wj} + u_{oj} \quad (2)$$

$$u_{Lj} = L_{\rm up} \frac{di_{uj}}{dt} + M_u \frac{di_{wj}}{dt} + L_{lw} \frac{di_{wj}}{dt} + M_u \frac{di_{uj}}{dt} \quad (3)$$

where u_{Lj} is the voltage across the coupled inductors, M_u is the mutual inductance, $R_{\rm up}, R_{lw}$ and $L_{\rm up}, L_{lw}$ are the resistances and self-inductances, respectively. It is assumed that the coupling coefficient of two windings equals 1 (i.e., $L_{\rm up} = L_{lw} = M_u = L_0$) and the resistances of the inductors are neglected for simplicity. Hence, the expressions (1)–(3) can be derived as

$$u_{oj} = \frac{1}{2}(u_{wj} - u_{uj}) \quad (4)$$

$$u_{Lj} = -u_{wj} - u_{uj} + E = 4L_0 \frac{di_{cj}}{dt} \quad (5)$$

where i_{cj} is defined as the circulating current of phase j, which circulates through both the upper and lower arms and can be given by

$$i_{cj} = \frac{1}{2}(i_{uj} + i_{wj}). \quad (6)$$

According to (5), the circulating current i_{cj} can be obtained by performing the following integration:

$$i_{cj} = I_{cj} + \int_0^t \frac{u_{Lj}}{4L_0} dt \quad (7)$$

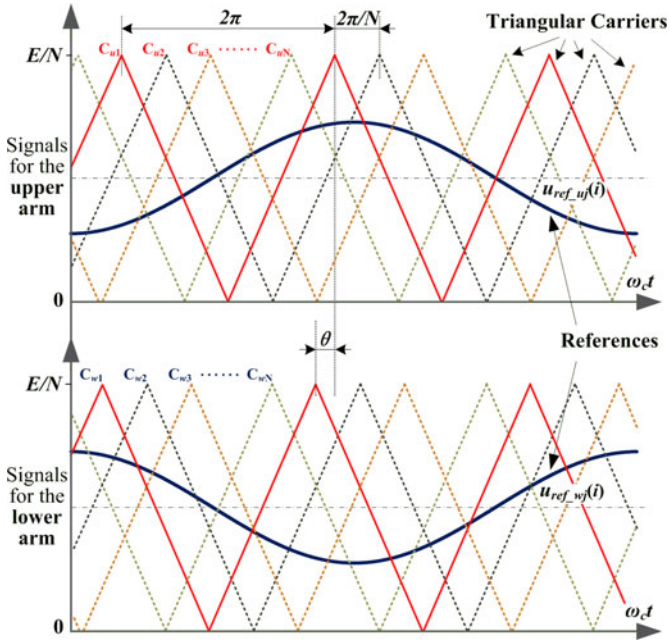

Fig. 3. PSC-PWM of MMC.

where I_{cj} is the dc component of the circulating current. Ideally, the phase current i_{oj} would be split equally between these two arms and the arm currents can be expressed as

$$i_{uj} = i_{cj} + \frac{1}{2} i_{oj} \tag{8}$$

$$i_{wj} = i_{cj} - \frac{1}{2} i_{oj}. \tag{9}$$

III. Implementation of PSC Modulation into MMCs

A. Description of the PSC Modulation for MMC

As depicted in Fig. 3, when applying the PSC modulation to an MMC with N SMs per arm, there should be a total of 2 N triangular carriers with the frequency of f_c (C_{u1}–C_{uN} for the upper arm, and C_{w1}–C_{wN} for the lower arm) and 2 N reference signals ($u_{\mathrm{ref}\_uj}(i)$ for the ith SM in the upper arm, and $u_{\mathrm{ref}\_wj}(i)$ for the ith SM in the lower arm, $i = 1, 2, \ldots, N$). Each SM is assigned with a specific reference signal and a triangular carrier, such that all SMs have the same switching frequency and the semiconductor stresses are evenly distributed. Then, the switching pulses of each SM are generated by comparing the reference signal with the corresponding carrier wave.

In order to achieve best harmonic cancellation features, the N triangular carriers of each arm are shifted by $2\pi/N$ incrementally [30]. Therefore, the phase angle $\theta_w(i)$ of the ith carrier C_{wi} in the lower arm can be given by

$$\theta_w(i) = \frac{2\pi}{N} \times (i-1). \tag{10}$$

As for the ith carrier C_{ui} in the upper arm, that is

$$\theta_u(i) = \theta + \frac{2\pi}{N} \times (i-1). \tag{11}$$

where θ is defined as the displacement angle between the upper and lower carriers. Note that θ has a significant impact on the harmonic features of MMC and will be discussed in Section IV. Due to symmetry, the range of θ can be obtained as $[0, \pi/N]$.

B. Capacitor Voltage Balancing Method

As the SMs of MMC are modulated independently under PSC-PWM, the voltage balancing of the capacitors can be achieved by adjusting the reference signal of each SM. Fig. 4 shows the complete block diagram of PSC-PWM for MMC combined with the capacitor voltage balancing method, in which the reference signals $u_{\mathrm{ref}\_wj}(i)$ and $u_{\mathrm{ref}\_uj}(i)$ are given by

$$u_{\mathrm{ref}\_wj}(i) = \frac{E}{2N}\left(1 + M\cos\left(\omega_o t + \varphi_j\right)\right) + \Delta u_{\mathrm{ref}\_wj}(i) \tag{12}$$

$$u_{\mathrm{ref}\_uj}(i) = \frac{E}{2N}\left(1 + M\cos\left(\omega_o t + \varphi_j + \pi\right)\right) + \Delta u_{\mathrm{ref}\_uj}(i) \tag{13}$$

where M ($0 \le M \le 1$) denotes the modulation depth, ω_o is the angular frequency of the output ac voltage, and φ_j is the phase angle. $\Delta u_{\mathrm{ref}\_wj}(i)$ and $\Delta u_{\mathrm{ref}\_uj}(i)$ represent the reference adjustment of each SM in the lower and the upper arm, respectively. These reference adjustments are intended for the voltage balancing control of the SMs and can be calculated as

$$\Delta u_{\mathrm{ref}\_wj}(i) = K_p\left(U_{\mathrm{avg}\_j} - U_{\mathrm{SM}\_wj}(i)\right) \times i_{cj} \tag{14}$$

$$\Delta u_{\mathrm{ref}\_uj}(i) = K_p\left(U_{\mathrm{avg}\_j} - U_{\mathrm{SM}\_uj}(i)\right) \times i_{cj} \tag{15}$$

where K_p denotes the proportional gain, $U_{\mathrm{SM}\_wj}(i)$ is the capacitor voltage of ith SM in the lower arm, while $U_{\mathrm{SM}\_uj}(i)$ is the capacitor voltage of ith SM in the upper arm. U_{avg_j} is the average voltage of all the $2N$ SM capacitors within phase j. Equations (14) and (15) indicate that for the SMs with voltages lower than the average voltage, the product of the adjustment voltage and the circulating current i_{cj} will form a positive power transfer to charge these SMs. In contrast, a negative power transfer will be generated to discharge the SMs with voltages higher than the average voltage. Detailed implementation of the proposed voltage balancing control method can be seen in Fig. 4.

IV. Harmonic Features of MMC with PSC Modulation

In this section, the double Fourier series based analysis [35] is presented to investigate how the displacement angle of PSC modulation will influence the harmonics of the output phase voltage and the circulating current of MMC. Moreover, the optimum displacement angles to minimize the voltage harmonics and to eliminate the circulating current harmonics are also proposed, respectively.

A. Influence of the Displacement Angle on Harmonics of Output Voltage and Circulating Current of MMC

In the following harmonic analysis, it is assumed that all the capacitor voltages are naturally balanced (i.e., $\Delta u_{\mathrm{ref}\_wj}(i) =$

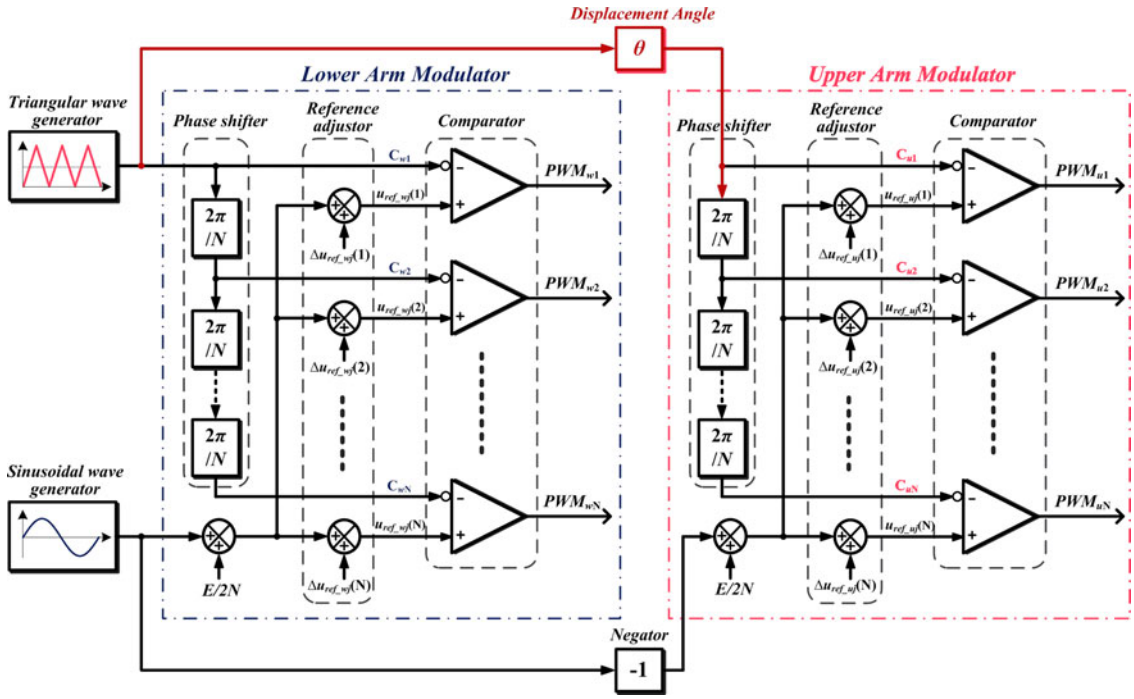

Fig. 4. Block diagram of the PSC-PWM applied to an MMC.

$\Delta u_{\mathrm{ref}\_uj}(i)=0$) thus the dc-link voltage E is equally distributed among the SMs (i.e., $U_{SM}=E/N$). Note that this assumption is reasonable because $\Delta u_{\mathrm{ref}\_wj}(i)$ and $\Delta u_{\mathrm{ref}\_uj}(i)$ are generally a relatively small portion when compared with $u_{\mathrm{ref}\_wj}(i)$ and $u_{\mathrm{ref}\_uj}(i)$, which can be proved by the experimental results in Section VI. Moreover, in normal operating conditions, the capacitance of each SM is always designed to limit the capacitor voltage fluctuations not exceeding 10% of the rated capacitor voltage. So for simplicity, the capacitance of each SM is supposed to be large enough so that the capacitor voltage fluctuations can be ignored.

According to (12), the Fourier representation of the output voltage of ith SM in the lower arm, $u_{wj}(i)$, can be expressed as

$$u_{wj}(i)=\frac{E}{2N}+\frac{ME}{2N}\cos(\omega_o t+\varphi_j)+\sum_{m=1}^{\infty}\sum_{n=-\infty}^{\infty}\frac{2E}{m\pi N}\times\sin\left[\frac{(m+n)\pi}{2}\right]\times J_n\left(\frac{M m\pi}{2}\right)\times\cos\left[m\left(\omega_c t+(i-1)\frac{2\pi}{N}\right)+n(\omega_o t+\varphi_j)\right] \tag{16}$$

where ω_c is the angular frequency of the triangular carriers, m is the harmonic order of the carrier wave ($m=1,\ldots,\infty$), n is the harmonic order of the reference wave ($n=-\infty,\ldots,-1,0,1,\ldots,\infty$), $J_n(x)$ refers to the Bessel coefficient of order n and argument x.

From (13), the output voltage of ith SM in the upper arm, $u_{uj}(i)$, can also be described by the same way

$$u_{uj}(i)=\frac{E}{2N}-\frac{ME}{2N}\cos(\omega_o t+\varphi_j)+\sum_{m=1}^{\infty}\sum_{n=-\infty}^{\infty}\frac{2E}{m\pi N}\times\sin\left[\frac{(m+n)\pi}{2}\right]\times J_n\left(\frac{M m\pi}{2}\right)\times\cos\left[m\left(\omega_c t+\theta+(i-1)\frac{2\pi}{N}\right)+n(\omega_o t+\varphi_j+\pi)\right]. \tag{17}$$

By summing the output voltages of N SMs, the arm voltages can be derived as

$$u_{wj}=\sum_{i=1}^{N}u_{wj}(i)=\frac{E}{2}+\frac{ME}{2}\cos(\omega_o t+\varphi_j)+\sum_{m=1}^{\infty}\sum_{n=-\infty}^{\infty}\frac{2E}{m\pi N}\sin\left[\frac{(Nm+n)\pi}{2}\right]\times J_n\left(\frac{MNm\pi}{2}\right)\cos\left[Nm\omega_c t+n(\omega_o t+\varphi_j)\right] \tag{18}$$

$$u_{uj}=\sum_{i=1}^{N}u_{uj}(i)=\frac{E}{2}-\frac{ME}{2}\cos(\omega_o t+\varphi_j)+\sum_{m=1}^{\infty}\sum_{n=-\infty}^{\infty}\frac{2E}{m\pi N}\sin\left[\frac{(Nm+n)\pi}{2}\right]\times J_n\left(\frac{MNm\pi}{2}\right)\cos\left[Nm(\omega_c t+\theta)+n(\omega_o t+\varphi_j+\pi)\right]. \tag{19}$$

Equations (18) and (19) show that all harmonics are eliminated except those at N-multiples of the carrier frequency and their sideband components.

Combining (4), (5), and (7) with (18) and (19), the output voltage and the circulating current of phase j can be obtained as (see Appendix A)

$$u_{oj} = \frac{1}{2}ME\cos(\omega_o t + \varphi_j) + \sum_{m=1}^{\infty}\sum_{n=-\infty}^{\infty}\frac{(-1)^n\,2E}{m\pi N} \times J_{2n+1-Nm}\left(\frac{MNm\pi}{2}\right) \times \cos\left[Nm\omega_c t + Q\right]\cos\left[\frac{Nm\,(\theta-\pi)}{2}\right] \tag{20}$$

$$i_{cj} = \frac{I_{\rm dc}}{3} - \sum_{m=1}^{\infty}\sum_{n=-\infty}^{\infty}\frac{(-1)^n\,E\times J_{2n+1-Nm}\,(MNm\pi/2)}{m\pi NL_0\,(Nm\omega_c+(2n+1-Nm)\,\omega_o)} \times \cos\left[Nm\omega_c t + Q\right]\sin\left[\frac{Nm\,(\theta-\pi)}{2}\right] \tag{21}$$

where

$$Q = (2n+1-Nm)\,(\omega_o t+\varphi_j) + \frac{Nm\,(\theta-\pi)}{2}. \tag{22}$$

It can be seen that the phase voltage u_{oj} and the circulating current i_{cj} both contain N-multiples of the carrier frequency harmonics with associated sideband components. Note that (21) focuses on the switching harmonics caused by PSC-PWM whereas not includes the low-frequency harmonics due to the energy oscillation between the upper and lower arms [9].

To analyze the impact of the displacement angle θ on the harmonic features, magnitudes of the *Nm*th carrier group harmonics of u_{oj} and i_{cj} are defined as $\hat{V}_{mn}$ and $\hat{I}_{mn}$, respectively. Therefore

$$\hat{V}_{mn} = K_{mn} \times \left|\cos\left[\frac{Nm\,(\theta-\pi)}{2}\right]\right| \tag{23}$$

$$\hat{I}_{mn} = H_{mn} \times \left|\sin\left[\frac{Nm\,(\theta-\pi)}{2}\right]\right| \tag{24}$$

where

$$K_{mn} = \frac{2E}{m\pi N}\left|J_{2n+1-Nm}\left(\frac{MNm\pi}{2}\right)\right| \tag{25}$$

$$H_{mn} = \frac{K_{mn}}{2L_0\,(Nm\omega_c + (2n+1-Nm)\,\omega_o)}. \tag{26}$$

Figs. 5 and 6 show the magnitudes of the *Nm*th carrier group harmonics of the output voltage and the circulating current as a function of displacement angle θ, respectively. Here, only the first six harmonic groups ($m \le 6$) are analyzed due to the limitation of this paper. It can be seen that for a particular harmonic group m, the voltage harmonic and the current harmonic are changed with θ at completely opposite tendency. It means that a minimum voltage harmonic is obtained at the cost of a maximum circulating current harmonic, and vice versa. Therefore, the displacement angle θ should be designed specifically according to the requirements of application conditions.

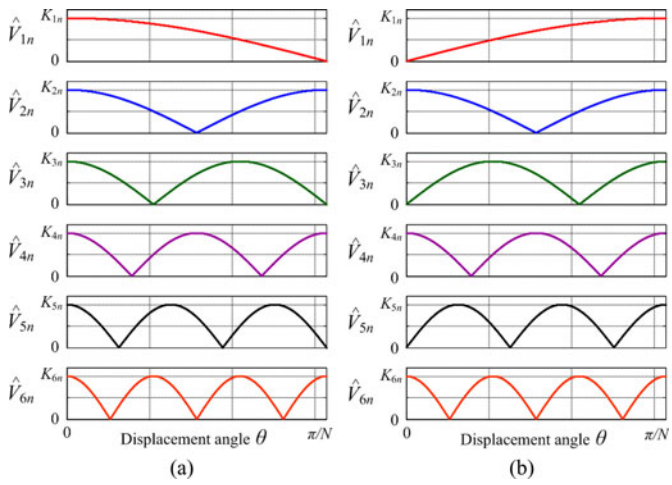

Fig. 5. Magnitudes of the harmonics of the phase output voltage at different displacement angles. (a) *N* is even. (b) *N* is odd.

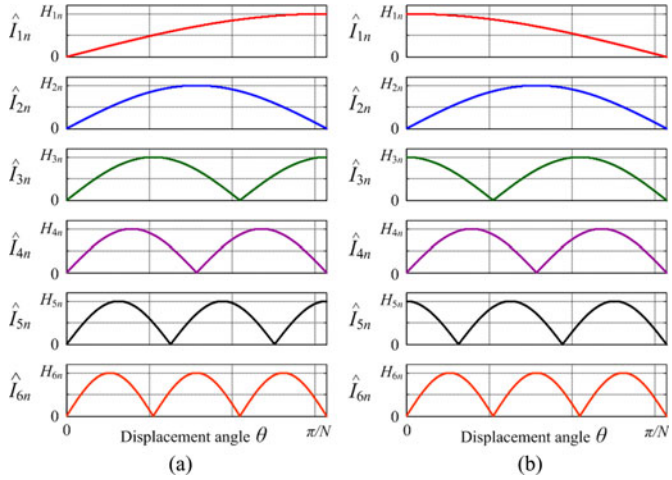

Fig. 6. Magnitudes of the harmonics of the phase circulating current at different displacement angles. (a) *N* is even. (b) *N* is odd.

B. Output Voltage Harmonics Minimization PSC Scheme

For most power converters, the output voltage with a higher resulting switching frequency and a lower harmonic distortion means smaller and lower-cost filters. Thus, from (23) and Fig. 5, the minimum voltage harmonics can be obtained in MMC by choosing the displacement angle as follows:

$$\theta = \begin{cases} 0, & N \text{ is odd} \\ \dfrac{\pi}{N}, & N \text{ is even} \end{cases}. \tag{27}$$

Then, the phase output voltage can be derived as

$$u_{oj} = \frac{1}{2}ME\cos(\omega_o t+\varphi_j) + \sum_{m=1}^{\infty}\sum_{n=-\infty}^{\infty}\frac{(-1)^{n+1}\,E}{m\pi N} \times J_{2n+1-2Nm}\,(MNm\pi)\cos\left[2Nm\omega_c t + Q'\right] \tag{28}$$

where Q' is given by

$$Q' = (2n+1-2Nm)\,(\omega_o t+\varphi_j)\,. \tag{29}$$

Evidently, voltage harmonics at odd multiples of the *Nm*th carrier group will be zero and the frequency of the lowest harmonic group rises to $2Nf_c$. Thus, the cutoff frequency of the output filter can be doubled, leading to a significant reduction of the filter size.

As for the circulating current at this displacement angle, even multiples of the *Nm*th carrier group harmonics are cancelled while odd multiples will reach their maximum values

$$\hat{I}_{mn} = H_{mn}, \qquad m = 1, 3, 5, ... \tag{30}$$

Note that these current harmonics will not only cause a lower efficiency of MMC, but apply a higher current stress upon the semiconductors. Moreover, if a smooth dc current is desired, extra filter must be added to the dc link in order to attenuate these current harmonics.

C. Circulating Current Harmonics Cancellation PSC Scheme

For MMC with a great number of SMs (e.g., in the HVDC application, N always equals several hundred), the THD of the output voltage itself will be extremely low and even no ac filters are needed. As a result, the harmonics of the circulating current become the main problem, which should be controlled at smaller magnitudes to reduce loss and the current stress. From (24) and Fig. 6, all the switching harmonics of the circulating current can be completely eliminated with the following displacement angle:

$$\theta = \begin{cases} \dfrac{\pi}{N}, & N \text{ is odd} \\ 0, & N \text{ is even} \end{cases}. \tag{31}$$

Under this condition, a pure circulating current can be achieved without unwanted switching harmonics thus the dc filters are not necessary anymore.

Meanwhile, with this displacement angle, the voltage harmonics are maximums

$$\hat{V}_{mn} = K_{mn}. \tag{32}$$

D. Harmonic Features of the Line-to-Line Voltage and DC-Link Current of MMC with PSC Modulation

For a three-phase MMC system, the reference signals of phase j ($j \in \{a, b, c\}$) can be obtained according to (12) and (13), where the phase angle is given by

$$\varphi_a = 0,\ \varphi_b = -\frac{2\pi}{3},\ \varphi_c = +\frac{2\pi}{3}. \tag{33}$$

From (20), the line-to-line output voltage can be calculated, that is

$$\begin{aligned} u_{ab} = u_{oa} - u_{ob} &= \frac{\sqrt{3}}{2} ME \cos\left(\omega_o t + \frac{\pi}{6}\right) \\ &+ \sum_{m=1}^{\infty} \sum_{n=-\infty}^{\infty} \frac{(-1)^n 4E}{m\pi N} \sin\left[Nm\omega_c t + Q''\right] \\ &\times J_{2n+1-Nm}\left(\frac{MNm\pi}{2}\right) \cos\left[\frac{Nm\left(\theta-\pi\right)}{2}\right] \\ &\times \sin\left[\frac{\left(2n+1-Nm\right)\pi}{3}\right] \end{aligned} \tag{34}$$

where

$$Q'' = \left(2n+1-Nm\right)\omega_o t + \frac{3Nm\theta - Nm\pi}{6} + \frac{\left(2n+1\right)\pi}{3}. \tag{35}$$

In this case, all the triplen sideband harmonics of u_{ab} are cancelled (i.e., $2n + 1 - Nm = 3, 6, 9, \ldots$) as the term of "sin [$(2n + 1 - Nm)\pi/3$]" in (34) is always zero. Based on (23), the line-to-line voltage magnitudes of the *Nm*th carrier group harmonics can be expressed as

$$\hat{V}_{ll\_mn} = \begin{cases} \sqrt{3}K_{mn}\left|\cos\left[\frac{Nm\left(\theta-\pi\right)}{2}\right]\right|, & \text{if } 2n+1-Nm \neq 0, 3, 6, \ldots \\ 0, & \text{else.} \end{cases} \tag{36}$$

Similarly, according to (21), the total dc-link current i_{dc} can also be obtained by summing the three phase circulating currents as

$$\begin{aligned} i_{\mathrm{dc}} &= \sum_{j=a,b,c} i_{cj} = I_{\mathrm{dc}} \\ &- \sum_{m=1}^{\infty} \sum_{n=-\infty}^{\infty} \frac{(-1)^n E \times J_{2n+1-Nm}\left(\frac{MNm\pi}{2}\right)}{m\pi NL_0\left(Nm\omega_c + \left(2n+1-Nm\right)\omega_o\right)} \\ &\times \cos\left[Nm\omega_c t + Q\right] \times \sin\left[\frac{Nm\left(\theta-\pi\right)}{2}\right] \\ &\times \left\{2\cos\left[\frac{\left(2n+1-Nm\right)2\pi}{3}\right] + 1\right\}. \end{aligned} \tag{37}$$

Contrary with the line-to-line voltage, all the sideband harmonics of the dc-link current are eliminated except those at triplen frequency. From (24), the magnitude of the *Nm*th carrier group harmonics of the dc-link current can be obtained as

$$\hat{I}_{\mathrm{dc}\_mn} = \begin{cases} 3H_{mn}\left|\sin\left[\frac{Nm\left(\theta-\pi\right)}{2}\right]\right|, & \text{if } 2n+1-Nm = 0, 3, 6, \ldots \\ 0, & \text{else.} \end{cases} \tag{38}$$

Note that (36) and (38) are still a function of displacement angle θ, the output voltage harmonics minimization and circulating current harmonics cancellation scheme as indicated above are also valid for the line-to-line voltage and dc-link current.

V. PSC Modulation for MMC with Full-Bridge SMs

Fig. 7 shows another SM configuration of MMC, the full-bridge structure [5], [6]. Although it needs double the number of semiconductors compared to half-bridge MMC, the full-bridge MMC can reverse the polarity of the dc-link voltage and has the ability to cut off the dc-side short-circuit current easily by turning off all the IGBTs [36]. In other words, full-bridge MMC is able to protect against dc network faults, which is an excellent characteristic especially in HVDC applications. Moreover, the full-bridge MMC can provide a boosted ac voltage which is higher than the dc-link voltage [34]. It is, therefore, also a very attractive topology for renewable power generation applications

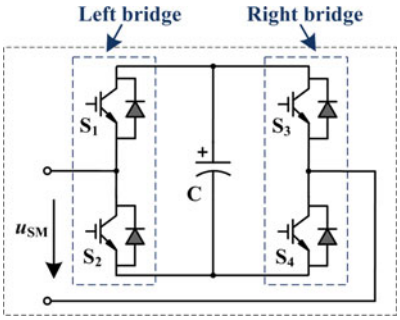

Fig. 7. Configuration of a full-bridge SM.

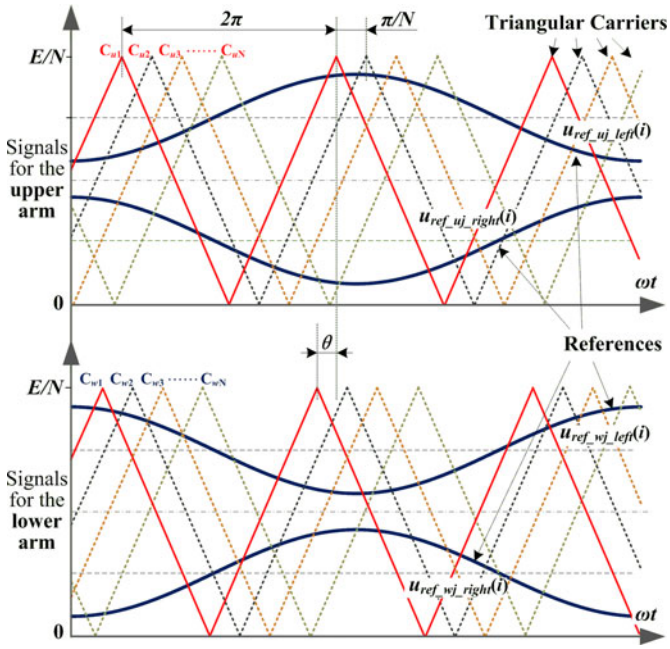

Fig. 8. PSC-PWM for MMC with full-bridge SMs.

where the dc-link voltage may vary in a wide range. In this section, an extension of the PSC modulation for MMC with full-bridge SMs is performed, and the optimum displacement angle to minimize the output voltage harmonics or to eliminate the circulating current is also deduced, respectively.

A. PSC for Full-Bridge MMC

As shown in Fig. 8, the proposed PSC-PWM scheme of the full-bridge MMC is basically the same as that of Fig. 3 except for the following two modifications. One is that the carriers in each arm are shifted by π/N and the range of the displacement angle θ now is changed to

$$0 \le \theta \le \frac{\pi}{2N}. \tag{39}$$

The other modification is that there are two reference signals for each SM, one for the left bridge and the other for the right bridge. With respect to the ith SM in the lower arm, these references are given by

$$\begin{cases} u_{\mathrm{ref}\_wj\_\mathrm{left}}(i) = \dfrac{3E}{4N} + \dfrac{ME}{4N}\cos\left(\omega_o t + \varphi_j\right) + \Delta u_{\mathrm{ref}\_wj}(i) \\ u_{\mathrm{ref}\_wj\_\mathrm{right}}(i) \\ \qquad = \dfrac{E}{4N} + \dfrac{ME}{4N}\cos\left(\omega_o t + \varphi_j + \pi\right) - \Delta u_{\mathrm{ref}\_wj}(i) \end{cases}. \tag{40}$$

Similarly, for the ith SM in the upper arm, that is

$$\begin{cases} u_{\mathrm{ref}\_uj\_\mathrm{left}}(i) = \dfrac{3E}{4N} + \dfrac{ME}{4N}\cos\left(\omega_o t + \varphi_j + \pi\right) + \Delta u_{\mathrm{ref}\_uj}(i) \\ u_{\mathrm{ref}\_uj\_\mathrm{right}}(i) = \dfrac{E}{4N} + \dfrac{ME}{4N}\cos\left(\omega_o t + \varphi_j\right) - \Delta u_{\mathrm{ref}\_uj}(i) \end{cases}. \tag{41}$$

Note that the capacitor voltage balancing method proposed in Section III for half-bridge MMCs is also effective for full-bridge MMCs and the reference adjustments $\Delta u_{\mathrm{ref}\_wj}(i)$ and $\Delta u_{\mathrm{ref}\_uj}(i)$ can still be obtained from (14) and (15).

Thus, the output voltage and circulating current of phase j can be obtained as (see Appendix B)

$$\begin{aligned} u_{oj} = {} & \frac{1}{2}ME\cos(\omega_o t + \varphi_j) + \sum_{m=1}^{\infty}\sum_{n=-\infty}^{\infty} \frac{(-1)^{Nm+n}\,2E}{m\pi N} \\ & \times J_{2n+1-Nm}\left(\frac{MNm\pi}{2}\right) \\ & \times \cos\left[2Nm\omega_c t + Q'''\right]\cos\left[Nm\left(\theta - \frac{\pi}{2}\right)\right] \end{aligned} \tag{42}$$

$$\begin{aligned} i_{cj} = {} & \frac{I_{\mathrm{dc}}}{3} \\ & - \sum_{m=1}^{\infty}\sum_{n=-\infty}^{\infty} \frac{(-1)^{Nm+n}\,E \times J_{2n+1-Nm}\left(MNm\pi/2\right)}{m\pi N L_0\left(2Nm\omega_c + (2n+1-Nm)\,\omega_o\right)} \\ & \times \sin\left[2Nm\omega_c t + Q'''\right]\sin\left[Nm\left(\theta - \frac{\pi}{2}\right)\right] \end{aligned} \tag{43}$$

where

$$Q''' = (2n+1-Nm)\left(\omega_o t + \varphi_j\right) + Nm\left(\theta - \frac{\pi}{2}\right). \tag{44}$$

Comparing (42) and (43) to (20) and (21), it can be perceived that full-bridge MMC can double the frequency of the harmonics of the output voltage as well as the circulating current, which means a much smaller filter can satisfy the same THD requirements.

B. Output Voltage Harmonics Minimization PSC Scheme

Similar with the derivation of (27), the output voltage harmonics minimization PSC scheme for full-bridge MMC is also valid by revising the displacement angle as

$$\theta = \begin{cases} 0, & N \text{ is odd} \\ \dfrac{\pi}{2N}, & N \text{ is even} \end{cases}. \tag{45}$$

In this way, the lowest harmonic frequency of the output voltage can increase to $4Nf_c$.

C. Circulating Current Harmonics Cancellation PSC Scheme

For full-bridge MMC, all the switching harmonics of the circulating current can also be eliminated when the displacement angle is selected as

$$\theta = \begin{cases} \dfrac{\pi}{2N}, & N \text{ is odd} \\ 0, & N \text{ is even} \end{cases}. \tag{46}$$

D. Comparison Between the Proposed PSC for Full-Bridge MMC and Traditional PSC for CHB

At first sight, the proposed PSC scheme for full-bridge MMC are quite similar with the traditional PSC scheme for CHB, as they are both dealing with the full-bridge SM and both capable of increasing the equivalent switching frequency. However, there are marked differences between these two PSC schemes, and it is imperative to reveal them: (It is supposed that MMC and CHB have the same number (2 N) of full-bridge SMs within one phase. As a result, each arm of MMC contains N SMs.)

1) Carrier differences. For full-bridge MMC, the carriers are distributed evenly among the N SMs within the same arm (upper or lower), with the phase shift of π/N. Meanwhile, there should be an interleaved displacement angle between the upper-arm and lower-arm carriers, which needs to be designed carefully to improve the output voltage (or the circulating current) harmonic features. However, since CHB does not have the dc terminal and therefore has no circulating current, the traditional PSC scheme to CHB only needs to take consideration of the output voltage harmonics, where the carriers are distributed equally among all the $2N$ SMs, with a phase shift of $\pi/2N$ [30].
2) Reference differences. It is easy to generate the references for CHB, as all the $2N$ SMs are modulated using the same sinusoidal reference. In contrast, with respect to MMC, the references should be classified into the upper and the lower arm, and a 1/4 dc voltage shift should also be introduced, as shown in (40) and (41).

VI. Experimental Results

In order to verify the validity of the mathematical analysis and the proposed PSC method, a three-phase MMC prototype with three SMs per arm has been built, as shown in Fig. 9. The circuit parameters and operating conditions are listed in Table I. It should be noted that each SM of this prototype contains four IGBTs so that both the half-bridge and the full-bridge SM configuration can be verified in this prototype.

As for the controller, a TMS320F28335 DSP is used to generate the three-phase sinusoidal references while an EP3C25Q240C8 FPGA is adopted to generate the triangular carriers as well as the reference adjustments for capacitor voltage balancing. Finally, the generated PWM signals are sent to SMs via optical fibers.

A. Experimental Results of MMC with Half-Bridge SMs

Figs. 10–14 show the experimental results of the prototype with half-bridge SMs. Fig. 10 presents the harmonic magnitudes

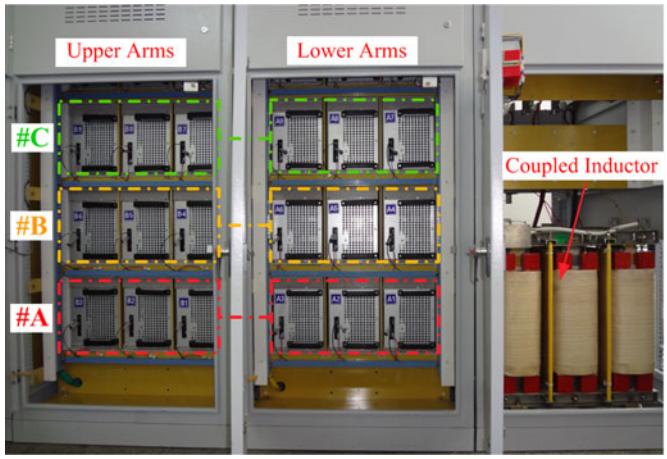

Fig. 9. Laboratory setup.

TABLE I
Circuit Parameters of the MMC Prototype

Quantity	Value
Number of SMs per arm	N=3
DC-link voltage	E=300V
Reference voltage frequency	f_o=50Hz
Rated SM capacitor voltage	U_{sm}=100V
SM capacitance	C_{sm}=1867μF
Buffer inductors	L_{up}=L_{lw}=M_u=0.8mH
Carrier frequency	f_c=1.017kHz
Modulation index	M=0.87
Load Resistance	R_{load}=20Ω
Load Inductance	L_{load}=1.5mH

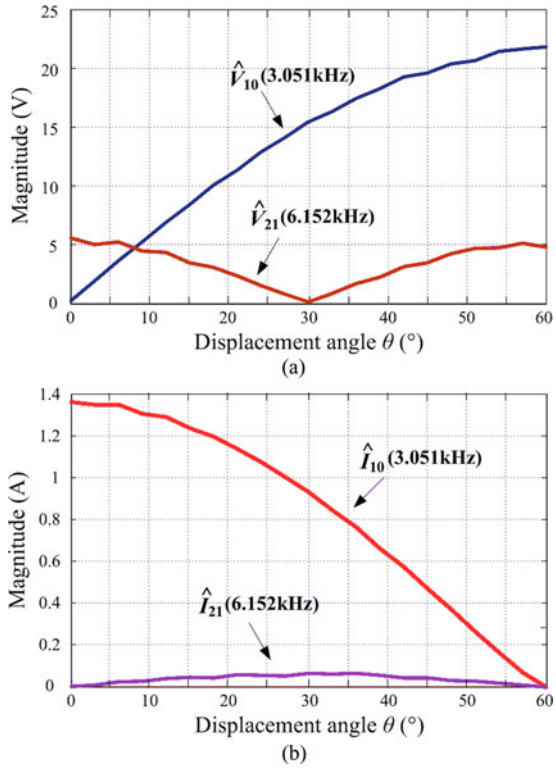

Fig. 10. Experimentally measured harmonic magnitudes with respect to θ: (a) harmonics of phase voltage and (b) harmonics of circulating current.

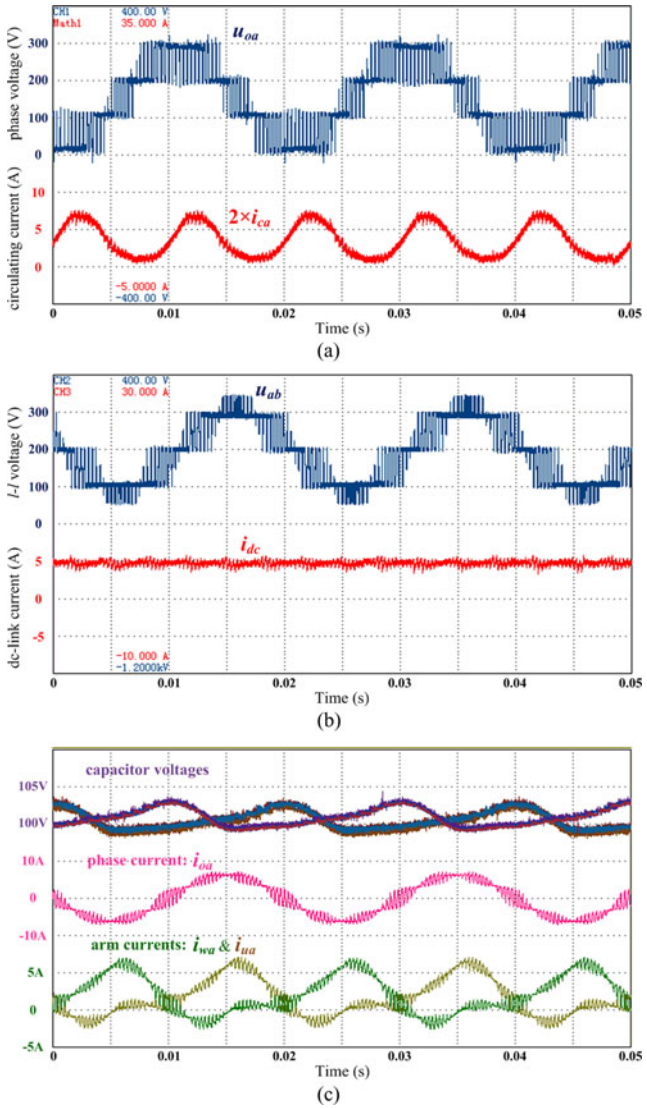

Fig. 11. Experimental waveforms of half-bridge MMC when applying the circulating current harmonics cancellation PSC-PWM: (a) phase voltage u_{oa} and circulating current i_{ca}, (b) line-to-line voltage u_{ab} and dc-link current i_{dc}, (c) SM capacitor voltages of phase a, phase current i_{oa}, lower arm current i_{wa}, and upper arm current i_{ua}.

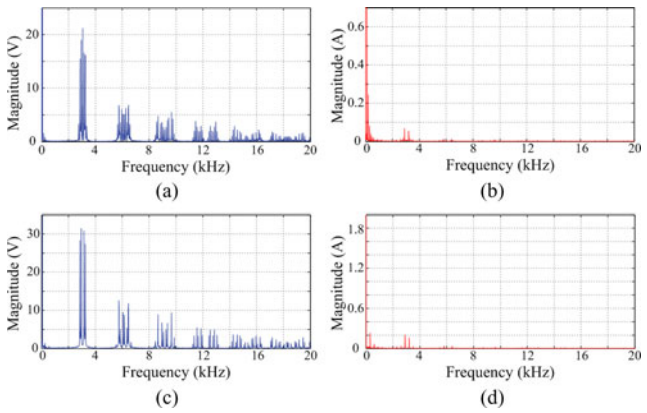

Fig. 12. Measured harmonic spectrums of half-bridge MMC when applying the circulating current harmonics cancellation PSC-PWM: (a) phase voltage u_{oa}, (b) circulating current i_{ca}, (c) line-to-line voltage u_{ab}, and (d) dc-link current i_{dc}.

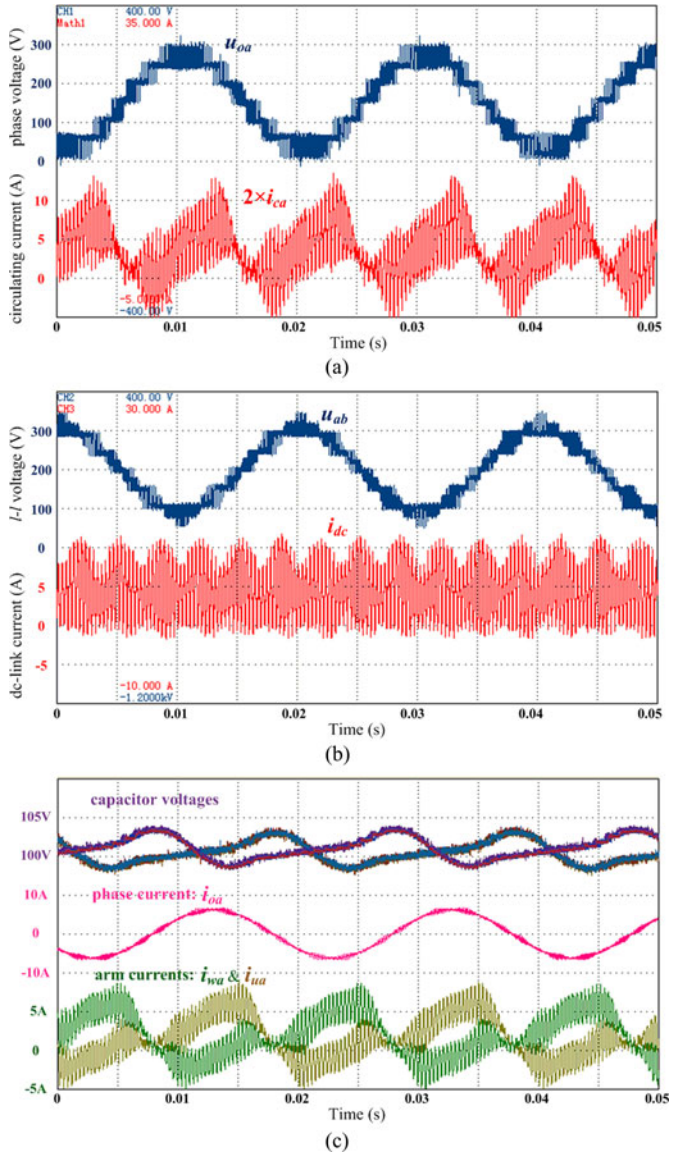

Fig. 13. Experimental waveforms of half-bridge MMC when applying the output voltage harmonics minimization PSC-PWM: (a) phase voltage u_{oa} and circulating current i_{ca}, (b) line-to-line voltage u_{ab} and dc-link current i_{dc}, (c) SM capacitor voltages of phase a, phase current i_{oa}, lower arm current i_{wa}, and upper arm current i_{ua}.

of the measured output phase voltage and the circulating current. These magnitudes are obtained by exporting the oscilloscope waveforms to MATLAB and calculated by using the built-in functions for discrete Fourier transform (i.e., "fft(x)"). Comparing Fig. 10 with Figs. 5(a) and 6(a), we can see that there is a reasonably good agreement between the analytical and the experimental curves. Please note that the measured magnitudes of the harmonics are slightly different from the analytically calculated values because of some non-ideal factors such as the dead-time effect and the propagation delay of optical fibers.

Figs. 11 and 12 present the experimental results with the circulating current harmonics cancellation PSC scheme, where the displacement angle is selected by (31) as $\theta = 60°$. It should be noted that the circulating current is obtained by the math

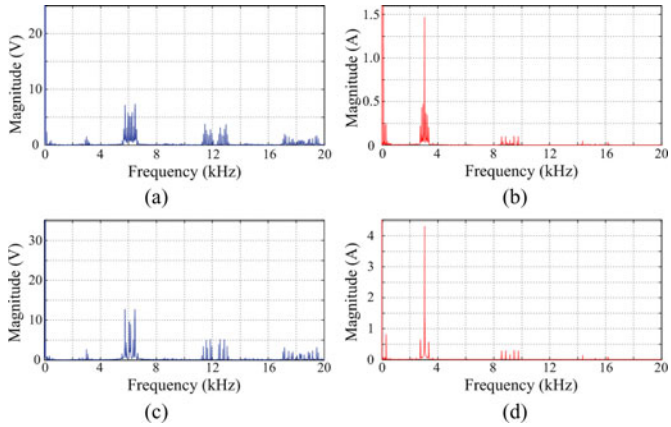

Fig. 14. Measured harmonic spectrums of half-bridge MMC when applying the output voltage harmonics minimization PSC-PWM: (a) phase voltage u_{oa}, (b) circulating current i_{ca}, (c) line-to-line voltage u_{ab}, (d) dc-link current i_{dc}.

function of an oscilloscope by adding the upper arm and the lower arm currents (i.e., $i_{ua} + i_{wa}$). Hence the magnitude of the circulating current waveform is multiplied by 2 (i.e., $2 \times i_{ca}$). As shown in Fig. 11, there are basically no switching harmonics in waveforms of the circulating current i_{ca} as well as the dc-link current i_{dc}, which can be proved by the harmonic spectrums in Fig. 12(b) and (d). Moreover, waveforms of u_{oa} and u_{ab} indicate that the phase voltage contains four voltage levels while the line-to-line voltage has seven levels. The spectra of u_{oa} and u_{ab} in Fig. 12(a) and (c) indicate that the equivalent switching frequency of the output voltage is about 3 kHz and there are less harmonic components in u_{ab} because of the triplen sideband harmonics cancellation between the phases. Fig. 11(c) shows the six SM capacitor voltages in the upper and lower arms of phase a. It can be seen that these capacitor voltages are kept balanced with the capacitor voltage balancing method.

Although a 5% voltage ripple of the capacitor voltages can be found in Fig. 12(c), the experimentally obtained harmonic spectrums still agree well with the theoretical analysis, which demonstrates the rationality of assuming an infinite SM capacitance during the analysis in Section IV. In addition, as the capacitor voltage ripples of the upper arm SMs and lower arm SMs are opposite, there is an energy oscillation between these two arms. As a result, we can see that i_{ca} and i_{dc} also both contain some low-frequency ripples (mainly second-order harmonic for i_{ca}, and sixth-order harmonic for i_{dc}). Note that these low-frequency current harmonics can be suppressed by increasing the inductance of the arm inductor or by adding additional control loops [19], [37]–[40].

Figs. 13 and 14 show the experimental results when applying the output voltage harmonics minimization PSC scheme, where $\theta = 0^\circ$ [see (27)]. Compared to Fig. 11, it is clear from Fig. 13 that the level number of u_{oa} is increased to 7 and that of u_{ab} is increased to 13, which means the voltage THD is apparently reduced. This can be confirmed by the harmonic spectrums in Fig. 14(a) and (c) that all the harmonics in the odd harmonic groups (i.e., 3 kHz, 9 kHz, 15 kHz, ...) have disappeared and the equivalent switching frequency of the output voltage rises to 6 kHz. The ripple of the phase current i_{oa} in Fig. 13(c) is

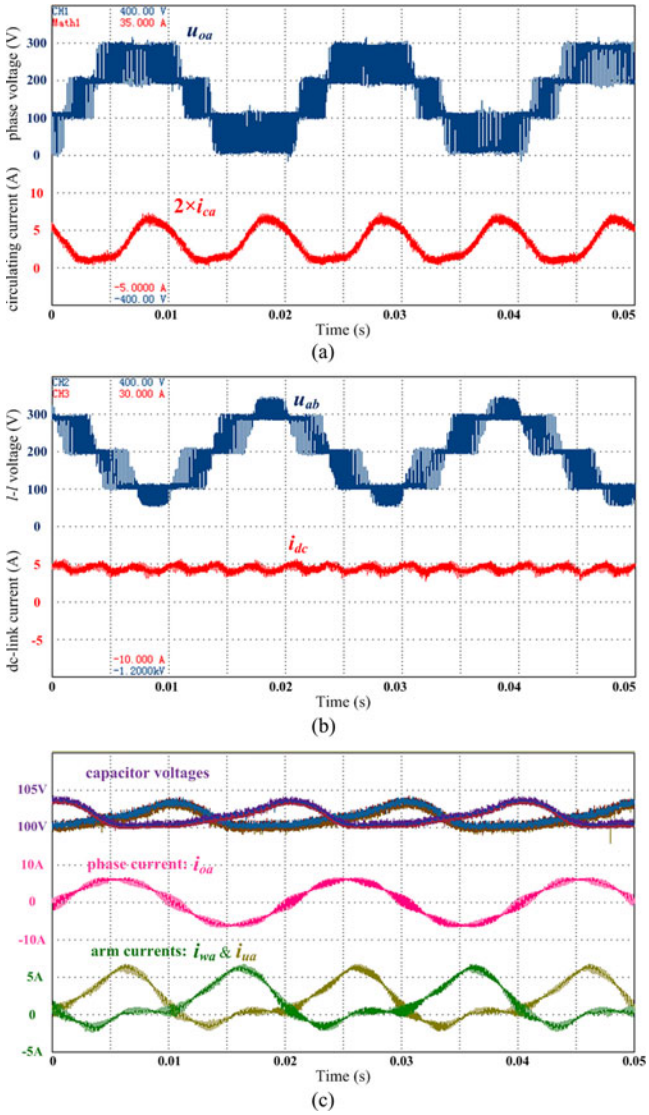

Fig. 15. Experimental waveforms of full-bridge MMC when applying the circulating current harmonics cancellation PSC-PWM, (a) phase voltage u_{oa} and circulating current i_{ca}, (b) line-to-line voltage u_{ab} and dc-link current i_{dc}, (c) SM capacitor voltages of phase a, phase current i_{oa}, lower arm current i_{wa}, and upper arm current i_{ua}.

apparently much smaller than that of Fig. 11(c). Meanwhile, as can be observed, there are significant switching ripples in the waveforms of i_{ca} and i_{dc}. Fig. 14(b) and (d) also show that i_{dc} contains less harmonic components than i_{ca} because only triplen sideband harmonics exist in i_{dc}. In addition, the capacitor voltages are also well balanced under this condition.

B. Experimental Results of MMC with Full-Bridge SMs

Experiments on the full-bridge MMC are also carried out in this research. The circuit parameters and operating conditions are exactly same as those in Figs. 11–14 while the only difference is that the half-bridge SMs are replaced by full-bridge SMs.

Figs. 15–18 show the experimental results of the full-bridge MMC. Note that the displacement angles of the output voltage

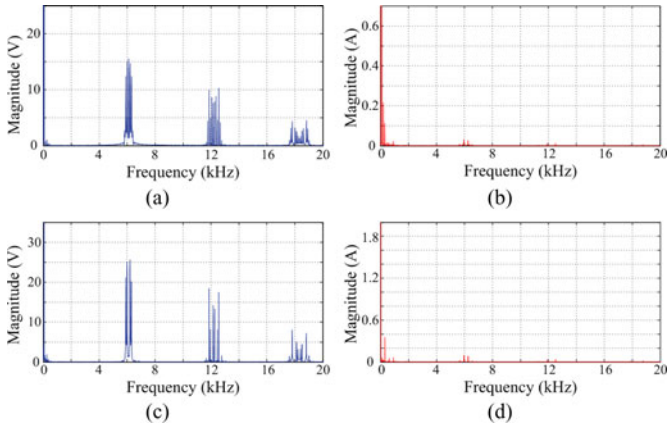

Fig. 16. Measured harmonic spectrums of full-bridge MMC when applying the circulating current harmonics cancellation PSC-PWM: (a) phase voltage u_{oa}, (b) circulating current i_{ca}, (c) line-to-line voltage u_{ab}, (d) dc-link current i_{dc}.

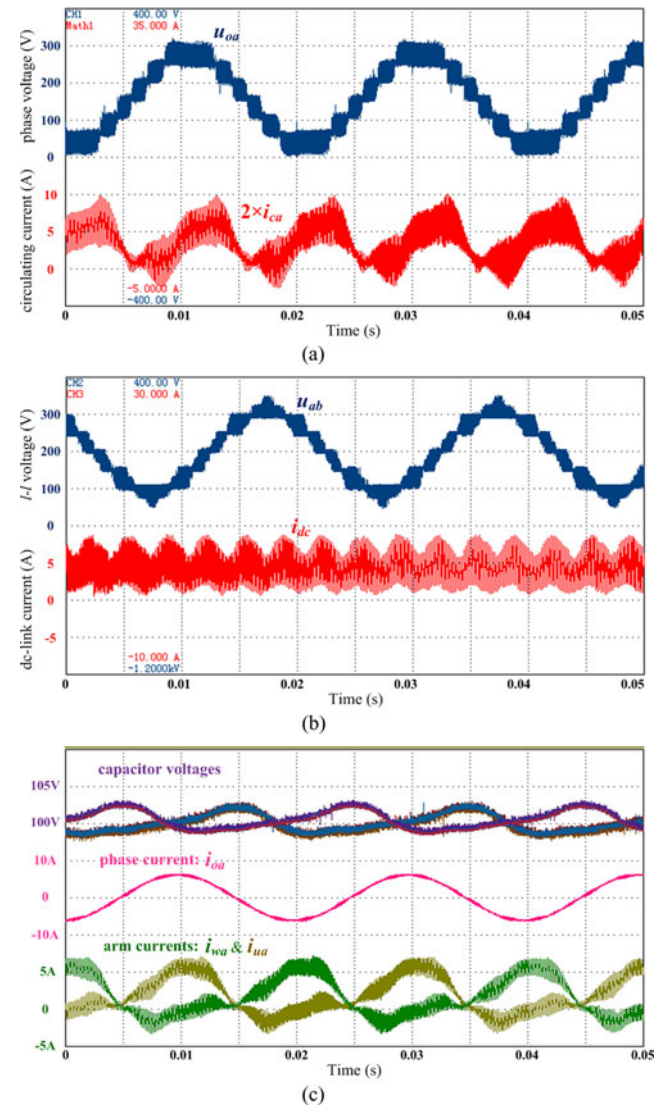

Fig. 17. Experimental waveforms of full-bridge MMC when applying the output voltage harmonics minimization PSC-PWM: (a) phase voltage u_{oa} and circulating current i_{ca}, (b) line-to-line voltage u_{ab} and dc-link current i_{dc}, (c) SM capacitor voltages of phase a, phase current i_{oa}, lower arm current i_{wa}, and upper arm current i_{ua}.

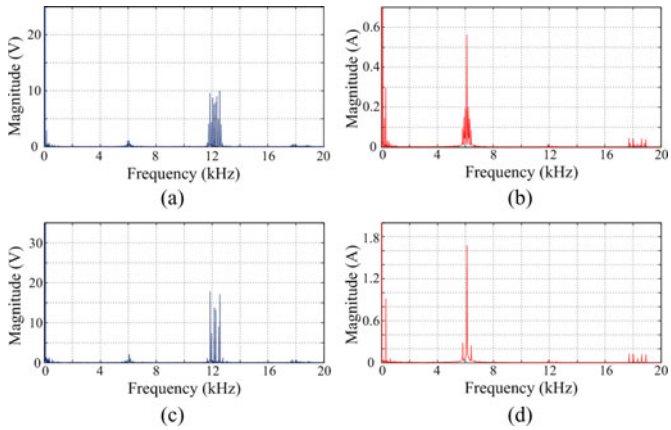

Fig. 18. Measured harmonic spectrums of full-bridge MMC when applying the output voltage harmonics minimization PSC-PWM: (a) phase voltage u_{oa}, (b) circulating current i_{ca}, (c) line-to-line voltage u_{ab}, (d) dc-link current i_{dc}.

harmonics minimization scheme and the circulating current harmonics cancellation PSC scheme for full-bridge MMC are calculated by (45) and (46), which are $\theta = 0°$ and $\theta = 30°$, respectively. It can be seen that the waveforms of full-bridge MMC are quite similar to those in Figs. 11 and 13 except they look much denser. This is due to the two times frequency increase of the switching harmonics of the output voltage as well as the circulating current (e.g., as shown in Fig. 18(a), the equivalent switching frequency of u_{oa} is around 12 kHz, which is twice as much as that in Fig. 14(a). Thus, one can notice that full-bridge MMC has better harmonic features than the half-bridge MMC and can reduce the size of both the dc-side and the ac-side filters. Moreover, it can be seen that the capacitor voltage balancing method is still effective for MMC with full-bridge SMs.

VII. Conclusion

This paper has presented a theoretical analysis of the PSC modulation for the MMC. Basic operating principles of PSC used in MMC and the corresponding capacitor voltage balancing method are introduced. The well-known Fourier series is utilized to quantify the harmonic features of the output voltage as well as the circulating current. Then, it is found that the harmonic magnitudes of the output voltage and the circulating current are functions of the displacement angle between the upper and lower arms. Based on the analysis, the optimum displacement angles to minimize the output voltage harmonics and to eliminate the switching harmonics of circulating current are identified, respectively. Furthermore, harmonic characteristics of the line-to-line voltage and the dc-link current are also developed. With respect to MMC with full-bridge SMs, an extension of the PSC scheme is also proposed which can increase the equivalent switching frequency and thus reduce the size of required filters.

The validity of the mathematical analysis and the proposed methods are confirmed by experiments based on a three-phase MMC prototype and we can draw the conclusion that the PSC modulation is a flexible and effective PWM solution for MMCs.

APPENDIX A

A. Derivation of (20) and (21)

Substituting (18) and (19) into (4) and (5) leads to

$$u_{oj}=\frac{1}{2}ME\cos(\omega_o t+\varphi_j)+\sum_{m=1}^{\infty}\sum_{n=-\infty}^{\infty}\frac{2E}{m\pi N}J_n\left(\frac{MNm\pi}{2}\right)\times\sin\left[\frac{(Nm+n)\pi}{2}\right]\times\sin\Big[Nm\omega_c t+n(\omega_o t+\varphi_j)+\frac{Nm\theta+n\pi}{2}\Big]\sin\left[\frac{Nm\theta+n\pi}{2}\right] \tag{A1}$$

$$u_{Lj}=-\sum_{m=1}^{\infty}\sum_{n=-\infty}^{\infty}\frac{4E}{m\pi N}J_n\left(\frac{MNm\pi}{2}\right)\sin\left[\frac{(Nm+n)\pi}{2}\right]\times\cos\left[Nm\omega_c t+n(\omega_o t+\varphi_j)+\frac{Nm\theta+n\pi}{2}\right]\times\cos\left[\frac{Nm\theta+n\pi}{2}\right]. \tag{A2}$$

Substituting (A2) into (7), the circulating current i_{cj} can be obtained as

$$i_{cj}=\frac{I_{\rm dc}}{3}-\sum_{m=1}^{\infty}\sum_{n=-\infty}^{\infty}\frac{E\times J_n\left(\frac{MNm\pi}{2}\right)}{m\pi NL_0\left(Nm\omega_c+n\omega_o\right)}\times\sin\left[\frac{(Nm+n)\pi}{2}\right]\times\sin\Big[Nm\omega_c t+n(\omega_o t+\varphi_j)+\frac{Nm\theta+n\pi}{2}\Big]\cos\left[\frac{Nm\theta+n\pi}{2}\right]. \tag{A3}$$

If "$Nm+n$" is even, the term of "sin [$(Nm+n)\pi/2$]" in (A1) and (A3) will be zero, leaving only $(2n+1-Nm)$th sideband harmonics of the Nmth carrier groups.

As a result, by modifying "n" into "$2n+1-Nm$," (A1) and (A3) can be presented as (20) and (21).

APPENDIX B

B. Derivation of (42) and (43)

Using the reference signals as given in (40), the output voltage of the left bridge of the ith SM in the lower arm, $u_{wj\_\rm left}(i)$ can be expressed by Fourier series as

$$u_{wj\_\rm left}(i)=\frac{3E}{4N}+\frac{ME}{4N}\cos(\omega_o t+\varphi_j)+\sum_{m=1}^{\infty}\sum_{n=-\infty}^{\infty}\frac{2E}{m\pi N}\times J_n\left(\frac{Mm\pi}{4}\right)\times\sin\left[\left(\frac{3m}{2}+n\right)\frac{\pi}{2}\right]\times\cos\left[m\left(\omega_c t+(i-1)\frac{\pi}{N}\right)+n(\omega_o t+\varphi_j)\right] \tag{B1}$$

and $u_{wj\_\rm right}(i)$ for the right bridge is

$$u_{wj\_\rm right}(i)=\frac{E}{4N}-\frac{ME}{4N}\cos(\omega_o t+\varphi_j)+\sum_{m=1}^{\infty}\sum_{n=-\infty}^{\infty}\frac{2E}{m\pi N}\times J_n\left(\frac{Mm\pi}{4}\right)\times\sin\left[\left(\frac{m}{2}+n\right)\frac{\pi}{2}\right]\times\cos\left[m\left(\omega_c t+(i-1)\frac{\pi}{N}\right)+n(\omega_o t+\varphi_j+\pi)\right]. \tag{B2}$$

Thus, the output voltage of the ith SM in the lower arm can then be obtained as

$$u_{wj}(i)=u_{wj\_\rm left}(i)-u_{wj\_\rm right}(i)=\frac{E}{2N}+\frac{ME}{2N}\cos(\omega_o t+\varphi_j)+\sum_{m=1}^{\infty}\sum_{n=-\infty}^{\infty}\frac{2E}{m\pi N}J_n\left(\frac{Mm\pi}{4}\right)\times\left\{\sin\left[\left(\frac{3m}{2}+n\right)\frac{\pi}{2}\right]-(-1)^n\sin\left[\left(\frac{m}{2}+n\right)\frac{\pi}{2}\right]\right\}\times\cos\left[m\left(\omega_c t+(i-1)\frac{\pi}{N}\right)+n(\omega_o t+\varphi_j)\right]. \tag{B3}$$

Once m is odd, $u_{wj}(i)$ is equal to zero. Then (B3) can be revised by replacing "m" with "$2m$," that is

$$u_{wj}(i)=\frac{E}{2N}+\frac{ME}{2N}\cos(\omega_o t+\varphi_j)+\sum_{m=1}^{\infty}\sum_{n=-\infty}^{\infty}\frac{E}{m\pi N}J_n\left(\frac{Mm\pi}{2}\right)\times\left\{\sin\left[(3m+n)\frac{\pi}{2}\right]-(-1)^n\sin\left[(m+n)\frac{\pi}{2}\right]\right\}\times\cos\left[2m\left(\omega_c t+(i-1)\frac{\pi}{N}\right)+n(\omega_o t+\varphi_j)\right]. \tag{B4}$$

Furthermore, if "$m+n$" is even, (B4) will also be zero. Thus, by modifying "n" into "$2n+1-m$," it becomes

$$u_{wj}(i)=\frac{E}{2N}+\frac{ME}{2N}\cos(\omega_o t+\varphi_j)+\sum_{m=1}^{\infty}\sum_{n=-\infty}^{\infty}\frac{(-1)^{m+n}\,2E}{m\pi N}\times J_{2n+1-m}\left(\frac{Mm\pi}{2}\right)\times\cos\Big[2m\left(\omega_c t+(i-1)\frac{\pi}{N}\right)+(2n+1-m)(\omega_o t+\varphi_j)\Big]. \tag{B5}$$

By summing the output voltages of N SMs, the lower arm voltage can be obtained as

$$u_{wj}=\sum_{i=1}^{N}u_{wj}(i)=\frac{E}{2}+\frac{ME}{2}\cos(\omega_o t+\varphi_j)+\sum_{m=1}^{\infty}\sum_{n=-\infty}^{\infty}\frac{(-1)^{Nm+n}\,2E}{m\pi N}J_{2n+1-Nm}\left(\frac{MNm\pi}{2}\right)\times\cos\left[2Nm\omega_c t+(2n+1-Nm)(\omega_o t+\varphi_j)\right]. \tag{B6}$$

Similarly, with the reference signals given in (41), the upper arm voltage can be expressed as

$$u_{uj} = \frac{E}{2} - \frac{ME}{2}\cos(\omega_o t + \varphi_j) + \sum_{m=1}^{\infty}\sum_{n=-\infty}^{\infty} \frac{(-1)^{Nm+n}\,2E}{m\pi N} \times J_{2n+1-Nm}\left(\frac{MNm\pi}{2}\right) \times \cos\Big[2Nm\omega_c t + 2Nm\theta + (2n+1-Nm)\,(\omega_o t + \varphi_j + \pi)\Big]. \tag{B7}$$

Thereby, substitution of (B6) and (B7) into (4) results in (42).

Substituting (B6) and (B7) into (5), the voltage across the coupled inductors u_{Lj} can be calculated as

$$u_{Lj} = -\sum_{m=1}^{\infty}\sum_{n=-\infty}^{\infty} \frac{(-1)^{Nm+n}\,2E}{m\pi N} J_{2n+1-Nm}\left(\frac{MNm\pi}{2}\right) \times \sin\left[Nm\left(\theta - \frac{\pi}{2}\right)\right] \times \sin\Big[2Nm\omega_c t + (2n+1-Nm)\,(\omega_o t + \varphi_j) + Nm\left(\theta - \frac{\pi}{2}\right)\Big]. \tag{B8}$$

Hence, substituting (B8) into (7) yields (43).

REFERENCES

[1] B. Bose, "Global energy scenario and impact of power electronics in 21st. century," *IEEE Trans. Ind. Electron.*, vol. 60, no. 7, pp. 2638–2651, Jul. 2013.

[2] I. Erlich, F. Shewarega, C. Feltes, F. W. Koch, and J. Fortmann, "Offshore wind power generation technologies," *Proc. IEEE*, vol. 101, no. 4, pp. 891–905, Apr. 2013.

[3] C. C. Davidson and G. De Preville, "The future of high power electronics in transmission and distribution power systems," presented at the 13th Eur. Conf. Power Electron. Appl. (EPE), Barcelona, Spain, Sep. 8–10, 2009.

[4] A. Lesnicar and R. Marquardt, "An innovative modular multilevel converter topology suitable for a wide power range," presented at the IEEE PowerTech. Conf., vol. 3, Bologna, Italy, Jun. 23–26, 2003.

[5] H. Akagi, "Classification, terminology, and application of the modular multilevel cascade converter (MMCC)," *IEEE Trans. Power Electron.*, vol. 26, no. 11, pp. 3119–3130, Nov. 2011.

[6] R. Marquardt, "Modular multilevel converter: An universal concept for HVDC-networks and extended DC-bus-applications," presented at the Int. Power Electron. Conf., Sapporo, Japan, Jun. 2010.

[7] J. Glasdam, J. Hjerrild, L. H. Kocewiak, and C. L. Bak, "Review on multilevel voltage source converter based HVDC technologies for grid connection of large offshore wind farms," in *Proc. PowerCon.*, 2012, vol. 1, pp. 79–84.

[8] K. Friderich, "Modern HVDC PLUS application of VSC in modular multilevel converter topology," in *Proc. Int. Symp. Ind. Electron.*, Jul. 2010, pp. 3807–3810.

[9] K. Ilves, A. Antonopoulos, S. Norrga, and H.-P. Nee, "Steady-state analysis of interaction between harmonic components of arm and line quantities of modular multilevel converters," *IEEE Trans. Power Electron.*, vol. 27, no. 1, pp. 57–68, Jan. 2012.

[10] A. Antonopoulos, L. Angquist, and H.-P. Nee, "On dynamics and voltage control of the modular multilevel converter," in *Proc. 13th Eur. Conf. Power Electron. Appl. (EPE)*, Barcelona, Spain, Sep. 8–10, 2009.

[11] L. Angquist, A. Antonopoulos, D. Siemazko, K. Ilves, M. Vasiladiotis, and H.-P. Nee, "Open-loop control of modular multilevel converters using estimation of stored energy," *IEEE Trans. Ind. Appl.*, vol. 47, no. 6, pp. 2516–2524, Nov./Dec. 2011.

[12] L. Harnefors, A. Antonopoulos, S. Norrga, L. Angquist, and H.-P. Nee, "Dynamic analysis of modular multilevel converters," *IEEE Trans. Ind. Electron.*, vol. 60, no. 7, pp. 2526–2537, Jul. 2013.

[13] U. N. Gnanarathna, A. M. Gole, and R. P. Jayasinghe, "Efficient modeling of modular multilevel HVDC converters (MMC) on electromagnetic transient simulation programs," *IEEE Trans. Power Del.*, vol. 26, no. 1, pp. 316–324, Jan. 2011.

[14] M. Guan and Z. Xu, "Modeling and control of a modular multilevel converter-based HVDC system under unbalanced grid conditions," *IEEE Trans. Power Electron.*, vol. 2, no. 12, pp. 4858–4867, Dec. 2012.

[15] D. Peftitsis, G. Tolstoy, A. Antonopoulos, J. Rabkowski, J.-K. Lim, M. Bakowski, L. Angquist, and H.-P. Nee, "High-power modular multilevel converters with SiC JFETs," *IEEE Trans. Power Electron.*, vol. 27, no. 1, pp. 28–36, Jan. 2012.

[16] S. Rohner, S. Bernet, M. Hiller, and R. Sommer, "Modulation, losses, and semiconductor requirements of modular multilevel converters," *IEEE Trans. Ind. Electron.*, vol. 57, no. 8, pp. 2633–2642, Aug. 2010.

[17] J. Qin and M. Saeedifard, "Predictive control of a modular multilevel converter for a back-to-back HVDC system," *IEEE Trans. Power Del.*, vol. 27, no. 3, pp. 1538–1547, Jul. 2012.

[18] M. Hagiwara and H. Akagi, "Control and experiment of pulsewidth modulated modular multilevel converters," *IEEE Trans. Power Electron.*, vol. 24, no. 7, pp. 1737–1746, Jul. 2009.

[19] Q. Tu, Z. Xu, and L. Xu, "Reduced switching-frequency modulation and circulating current suppression for modular multilevel converters," *IEEE Trans. Power Del.*, vol. 26, no. 3, pp. 2009–2017, Jul. 2011.

[20] M. Hagiwara and H. Akagi, "Control and analysis of the modular multilevel cascade converter based on double-star chopper-cells (MMCC-DSCC)," *IEEE Trans. Power Electron.*, vol. 26, no. 6, pp. 1649–1658, Jun. 2011.

[21] S. Du, J. Liu, and J. Lin, "Leg-balancing control of the DC-link voltage for modular multilevel converters," *J. Power Electron.*, vol. 12, no. 5, pp. 739–747, 2012.

[22] E. Solas, G. Abad, J. Barrena, S. Aurtenetxea, A. Carcar, and L. Zajac, "Modular multilevel converter with different submodule concepts—Part I: Capacitor voltage balancing method," *IEEE Trans. Ind. Electron.*, vol. 60, no. 10, pp. 4525–4535, Oct. 2013.

[23] E. Solas, G. Abad, J. Barrena, S. Aurtenetxea, A. Carcar, and L. Zajac, "Modular multilevel converter with different submodule concepts—Part II: Experimental validation and comparison for HVDC application," *IEEE Trans. Ind. Electron.*, vol. 60, no. 10, pp. 4536–4545, Oct. 2013.

[24] Q. Tu and Z. Xu, "Impact of sampling frequency on harmonic distortion for modular multilevel converter," *IEEE Trans. Power Del.*, vol. 26, no. 1, pp. 298–306, Jan. 2011.

[25] K. Ilves, A. Antonopoulos, S. Norrga, and H.-P. Nee, "A new modulation method for the modular multilevel converter allowing fundamental switching frequency," *IEEE Trans. Power Electron.*, vol. 27, no. 8, pp. 3482–3494, Aug. 2012.

[26] Z. Li, P. Wang, H. Zhu, Z. Chu, and Y. Li, "An improved pulse width modulation method for chopper-cell-based modular multilevel converters," *IEEE Trans. Power Electron.*, vol. 27, no. 8, pp. 3472–3481, Aug. 2012.

[27] G. P. Adam, O. Anaya-Lara, G. M. Burt, D. Telford, B. W. Williams, and J. R. McDonald, "Modular multilevel inverter: Pulse width modulation and capacitor balancing technique," *IET Power Electron.*, vol. 3, no. 5, pp. 702–715, Sep. 2010.

[28] M. Saeedifard and R. Iravani, "Dynamic performance of a modular multilevel back-to-back HVDC system," *IEEE Trans. Power Del.*, vol. 25, no. 4, pp. 2903–2912, Oct. 2010.

[29] S. Kouro, M. Malinowski, K. Gopakumar, J. Pou, L. G. Franquelo, B. Wu, J. Rodriguez, M. A. Perez, and J. I. Leon, "Recent advances and industrial applications of multilevel converters," *IEEE Trans. Ind. Electron.*, vol. 57, no. 8, pp. 2553–2580, Aug. 2010.

[30] D. G. Holmes and B. P. McGrath, "Opportunities for harmonic cancellation with carrier-based PWM for a two-level and multilevel cascaded inverters," *IEEE Trans. Ind. Appl.*, vol. 37, no. 2, pp. 574–582, Mar./Apr. 2001.

[31] R. Naderi and A. Rahmati, "Phase-shifted carrier PWM technique for general cascaded inverters," *IEEE Trans. Power Electron.*, vol. 23, no. 3, pp. 1257–1269, May. 2008.

[32] H. Peng, M. Hagiwara, and H. Akagi, "Modeling and analysis of switching-ripple voltage on the DC link between a diode rectifier and a modular multilevel cascade inverter (MMCI)," *IEEE Trans. Power Electron.*, vol. 28, no. 1, pp. 75–84, Jan. 2013.

[33] A. Shojaei and G. Joos, "An improved modulation scheme for harmonic distortion reduction in modular multilevel converter," in *Proc. IEEE Power Energy Soc. Gen. Meeting*, Jul. 2012, pp. 1–7.

[34] N. Thitichaiworakorn, M. Hagiwara, and H. Akagi, "Experimental verification of a modular multilevel cascade inverter based on double-star

bridge-cells (MMCI-DSBC)," *IEEE Trans. Ind. Appl.*, vol. 50, no. 1, pp. 509–519, Jan./Feb. 2014.
[35] D. G. Holmes and T. A. Lipo, *Pulse Width Modulation for Power Converters*. Piscataway, NJ, USA: IEEE Press, 2003, pp. 99–104.
[36] G. Adam, K. Ahmed, N. Singh, S. Finney, and B. Williams, "H-bridge modular multilevel converter (M2 C) for high-voltage applications," in *Proc. 21st Int. Conf. Exhib. Electricity Distribution*, Jun. 2011.
[37] M. Zhang, L. Huang, W. Yao, and Z. Lu, "Circulating harmonic current elimination of a CPS-PWM-based modular multilevel converter with a plug-in repetitive controller," *IEEE Trans. Power Electron.*, vol. 29, no. 4, pp. 2083–2097, Apr. 2014.
[38] M. Vasiladiotis, N. Cherix, and A. Rufer, "Accurate capacitor voltage ripple estimation and current control considerations for grid-connected modular multilevel converters," *IEEE Trans. Power Electron.*, to be published.
[39] Z. Li, P. Wang, Z. Chu, H. Zhu, Y. Luo, and Y. Li, "An inner current suppressing method for modular multilevel converters," *IEEE Trans. Power Electron.*, vol. 28, no. 11, pp. 4873–4879, Nov. 2013.
[40] G. Bergna, E. Berne, P. Egrot, P. Lefranc, A. Arzande, J. Vannier, and M. Molinas, "An energy-based controller for HVDC modular multilevel converter in decoupled double synchronous reference frame for voltage oscillations reduction," *IEEE Trans. Ind. Electron.*, vol. 60, no. 6, pp. 2360–2371, Jun. 2013.

Binbin Li was born in 1989. He received the B.S. and M.S. degrees in electrical engineering in 2010 and 2012, respectively, from the Harbin Institute of Technology, Harbin, China, where he is currently working toward the Ph.D. degree.

His current research interests include high-power electronics, multilevel converters, control algorithms, and PWM techniques.

Rongfeng Yang received the B.S., M.S., and Ph.D. degrees all in engineering physics from the Tsinghua University, Beijing, China, in 2001, 2003, and 2006, respectively.

In 2006, he joined the Department of Electrical Engineering, Harbin Institute of Technology, Harbin, China, as a Lecturer, where he finished the postdoctoral work. His current research interests include sensorless induction motors control and high-power medium-voltage application.

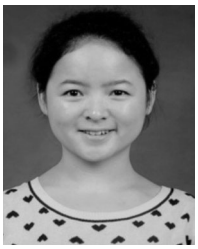

Dandan Xu was born in Xinjiang, China, in 1990. She received the B.S. degree in electrical engineering in 2013 from Harbin Institute of Technology, Harbin, China, where she is currently working toward the M.S. degree.

Her current research interests include modular multilevel converter.

Gaolin Wang (M'13) received the B.S., M.S., and Ph.D. degrees in electrical engineering from Harbin Institute of Technology, Harbin, China, in 2002, 2004, and 2008, respectively.

In 2009, he joined the Department of Electrical Engineering, Harbin Institute of Technology, as a Lecturer, where he has been an Associate Professor of Electrical Engineering since 2012. From 2009 to 2012, he was a Postdoctoral Fellow in Shanghai STEP Electric Corporation. He has authored or coauthored more than 30 technical papers published in journals and conference proceedings. He is the holder of seven Chinese patents. His current research interests include permanen-magnet synchronous motor drives, high-performance direct drive for traction system, position sensorless control of ac motors, and efficiency optimization control of interior PMSM.

Wei Wang was born in Heilongjiang Province, China, in 1963. She received the B.S. degree in automatic test and control, the M.S. degree in electrical engineering, and the Ph.D. degree in mechanical electronic engineering from Harbin Institute of Technology, Harbin, China, in 1984, 1990, and 2002, respectively.

Since 2003, she has been a Professor with the Department of Electrical Engineering, Harbin Institute of Technology. Her current research interests include soft-switching converters, digital control electronic ballast, and regenerative energy converter technique.

Dianguo Xu (M'97–SM'12) received the B.S. degree in control engineering from Harbin Engineering University, Harbin, China, in 1982, and the M.S. and Ph.D. degrees in electrical engineering from Harbin Institute of Technology (HIT), Harbin, China, in 1984 and 1989, respectively.

In 1984, he joined the Department of Electrical Engineering, HIT, as an Assistant Professor, where he has been a Professor since 1994. He was the Dean of School of Electrical Engineering and Automation, HIT, from 2000 to 2010. He is currently the Assistant President of HIT. His current research interests include renewable energy generation technology, multiterminal HVDC system based on VSC, power quality mitigation, speed sensorless vector-controlled motor drives, and high-performance PMSM servo system. He has authored or coauthored over 600 technical papers.

Dr. Xu is an Associate Editor for the IEEE TRANSACTIONS ON INDUSTRIAL ELECTRONICS. He is the Chairman of the IEEE Harbin Section, the Director of Lighting Power Supply Committee of CPSS, the Vice-director of Electric Automation Committee of CAA, Electrical Control System and Equipment Committee of CES, and Power Electronics Committee of CES.